https://doi.org/10.5194/egusphere-2026-3630
Preprint. Discussion started: 9 July 2026

Anthropogenic control on solar-induced hydro-meteorological summer extremes

Tobias Spiegl[1]*, Norel Rimbu[1], Franziska Kappenberger[2], Xiaojie Hao[3,1], Wenjuan Huo[4], Stephan Thober[5], Ulrike Langematz[2] and Gerrit Lohmann[1]

[1]Paleoclimate dynamics, Alfred-Wegener-Institut, Bremerhaven, Germany
[2]Freie Universität Berlin, Institut für Meteorologie, Berlin, Germany
[3]Frontiers Science Center for Deep Ocean Multispheres and Earth System and Key Laboratory of Physical Oceanography, Ocean University of China, Qingdao, China
[4]GEOMAR Helmholtz Centre for Ocean Research, Kiel, Germany
[5]Computational Hydrosystems Department, UFZ Leipzig, Germany
*Corresponding author: tobias.spiegl@awi.de

Abstract. Solar variability leaves detectable, climate state–dependent imprints on summer hydro-meteorological extremes. We show that centennial-scale solar minima, including the Maunder and Dalton minima, enhanced summer flooding and heavy precipitation from Western to Southeastern Europe under pre-industrial conditions, by combining a chemistry–climate model with palaeoclimate reconstructions and proxy records. We identify the physical mechanism linking reduced solar irradiance, stratospheric ozone changes, and sea-ice persistence to modified meridional temperature and pressure gradients and a southward shift of the European storm track. Model–data convergence supports this mechanism and its intra-seasonal amplification toward late summer. In a high-emissions future climate, the loss of summer sea ice and a weaker, northward-shifted storm track suppress this pathway, diminishing the sensitivity of European summer extremes to identical solar perturbations. Our results highlight the critical role of background climate state for interpreting solar fingerprints in past records and assessing future risks.

1 Introduction

The Sun, the key external climate driver, affects Earth's energy balance and atmospheric composition, with variations occurring on different timescales (Coddington et al., 2019). Short-term fluctuations in solar output, such as the 11-year solar cycle, induce subtle yet discernible imprints on Earth's climate system (Gray et al., 2010), although these effects remain challenging to isolate and quantify (Chiodo et al., 2019; Huo et al., 2025; Spiegl et al., 2023). In contrast, longer-term solar variations operating on centuries, such as Grand Solar Minima (GSM), have a documented influence on the climate (Ahmed et al., 2013). Anomalies in the content of cosmogenic 14C in different paleo-archives reveal at least 27 GSMs during the Holocene (Usoskin et al., 2007). Recent trends in solar activity over the past several solar cycles suggest the possibility of a

https://doi.org/10.5194/egusphere-2026-3630
Preprint. Discussion started: 9 July 2026

future return to GSM conditions (De Jager et al., 2016; Miyahara et al., 2021; Zolotova and Ponyavin, 2014). The Maunder Minimum (MM; 1645–1715) marks the last deep GSM and remains a key period for understanding past climate variability and anticipating future changes (Eddy, 1976; Luterbacher et al., 2001), yet the summer season has been much less studied than the boreal winter.

Several modelling studies have already examined how a future GSM or reduced future solar activity could influence climate change. These studies show that a strong future reduction in solar activity would not stop anthropogenic warming, but would only slightly reduce or delay it. Their main focus has been on long-term mean changes in temperature, radiative forcing, atmospheric chemistry, stratospheric ozone, and large-scale circulation under future greenhouse-gas scenarios (Feulner and Rahmstorf, 2010; Anet et al., 2013; Meehl et al., 2013; Ineson et al., 2015; Maycock et al., 2015; Arsenovic et al., 2018; Spiegl and Langematz, 2020; Sedlacek et al., 2023). Thus, previous work has mainly asked how much a future GSM or weakened solar forcing could modify the mean climate response to increasing greenhouse gases.

Our study fundamentally differs from these previous investigations in both scope and diagnostic focus. We do not focus on whether a future GSM could compensate for global warming in the long-term mean. Instead, we ask whether the same GSM-like solar perturbation produces the same regional climate response under different background climate states. In particular, we focus on hydro-meteorological summer extremes on synoptic timescales, because these short-lived weather events are often more relevant for societal impacts than seasonal or annual mean anomalies.

In this context, we show that reduced solar output during the MM and the Dalton Minimum (DM; 1790–1830) contributed to the occurrence of extreme hydro-meteorological summer events in Europe. We support this finding through a robust convergence of sediment records, high-resolution meteorological reconstructions (Rimbu et al., 2024), and targeted simulations with a state-of-the-art chemistry–climate model (Jöckel et al., 2010). Based on our model integrations, we propose a physical mechanism linking solar variability to summer extremes via a cascade of interactions involving solar radiation, stratospheric ozone, sea-ice and storm track dynamics under preindustrial climate conditions. Finally, we assess whether this mechanism remains active in a climate system increasingly dominated by anthropogenic forcing. Thus, our study provides a distinct perspective on solar–climate interactions: rather than quantifying the mean cooling effect of a future GSM, we test how centennial-scale solar forcing is translated into daily weather extremes, and how this translation changes between past and future climate conditions.

2 Materials and Methods

2.1 Model description

The EMAC (ECHAM/MESSy Atmospheric Chemistry) model—specifically ECHAM5 version 5.3.02 coupled with MESSy version 2.52—is a comprehensive chemistry-climate model developed to simulate atmospheric processes in the troposphere and middle atmosphere, while accounting for interactions with the ocean, sea ice, land surface, and anthropogenic influences

https://doi.org/10.5194/egusphere-2026-3630
Preprint. Discussion started: 9 July 2026

(Jöckel et al., 2010). EMAC leverages the Modular Earth Submodel System (MESSy2), which integrates contributions from multiple research institutions. Its atmospheric core is based on the ECHAM5 general circulation model (Roeckner et al., 2006). The model was configured in the T42L47MA setup, featuring a horizontal resolution of approximately 2.8° × 2.8° and 47 atmospheric layers, extending up to 0.01 hPa. Key submodules used in this configuration include MECCA for simulating atmospheric chemistry (Sander et al., 2011), JVAL for calculating photolysis rates (Sander et al., 2014), and a reduced-complexity tropospheric chemistry scheme to ensure computational efficiency. While the stratosphere and mesosphere follow the detailed CCMI-base-02 chemical mechanism (Jöckel et al., 2016), the compact chemistry in the lower atmosphere enables faster model runs without major compromises in accuracy. The chemical setup comprises 98 tracers and 156 reactions, of which 50 are photolytic. Additional components incorporated into the simulation include QBO (Giorgetta and Bengtsson, 1999) for simulating the quasi-biennial oscillation, UBCNOx (Funke et al., 2016) to represent auroral nitrogen oxide production, and MPIOM which incorporates dynamical coupling between the atmosphere, ocean and sea ice (Jungclaus et al., 2006) run at GR15L40 resolution (1.5° grid with 40 ocean levels). To enhance spectral accuracy in the ultraviolet and visible ranges, the FUBRAD module (Kunze et al., 2014) was employed in the stratosphere and mesosphere (below 70 hPa). It includes 81 spectral bands that capture key regions of the solar spectrum, such as the Lyman-α line (121.5 nm), Schumann–Runge bands (125.5–205 nm), Herzberg continuum (206.2–243.9 nm), Hartley bands (243.9–277.8 nm), Huggins bands (277.8–362.5 nm), and Chappuis bands (407.5–690 nm).

2.2 Experimental design

Two reference simulations were conducted with fixed solar radiation (based on the CMIP6 piControl solar forcing (Matthes et al., 2017)), alongside greenhouse gas and ODS concentrations corresponding to the years 1850 and 2100. In addition, two further simulations were performed, where the atmospheric composition mirrored that of the reference simulations, but a substantial reduction in solar radiation was applied. This solar reduction scenario simulates a strong decline in solar energy similar to the MM, based on the scenario described by McCracken and Beer (Egorova et al., 2018). As with the reference simulations, a constant GSM solar forcing was applied. To define this, we calculated the arithmetic mean of the reconstructed MM years (1690–1710) and used the results (for both TSI and SSI) as boundary conditions. All simulations were initialized from a historical simulation at the years 1850 and 2100. Once the global mean surface temperature reached equilibrium, each model run was extended for an additional 150 years. These years are the basis for the presented results.

2.3 Meteorological reconstructions

To reconstruct the R10mm index (i.e. the number of days with daily precipitation of at least 10 mm) anomaly field over the past six centuries, an established statistical methodology was employed (Rimbu et al., 2025). The summer season R10mm field, derived from the E-OBS observational dataset (Cornes et al., 2018) for the period 1950–2020, was first subjected to a

https://doi.org/10.5194/egusphere-2026-3630
Preprint. Discussion started: 9 July 2026

linear detrending procedure. Anomalies were defined as deviations from the climatological mean over this reference period. Subsequently, the R10mm anomaly field was decomposed via Empirical Orthogonal Function (EOF) analysis (von Storch and Zwiers, 2002). Predictors for the leading ten principal components (PCs) of R10mm were identified within the observed summer mean anomaly fields of temperature (Vose et al., 2021) and precipitation (Rustemeier et al., 2022), based on stability correlation criteria. Multiple linear regression models were then constructed for each of the ten PCs using the corresponding sets of selected temperature (T) and precipitation (PP) predictors. Based on models developed for the calibration period 1950–2020, we reconstruct the R10mm field back to 1900 using observed temperature (Vose et al., 2021) and precipitation (Rustemeier et al., 2022) as predictors. The reconstructed fields are validated against R10mm estimates derived from observational data sets (e.g. Dunn et al., 2020) and different reanalysis products (e.g. Slivinski et al., 2019), showing robust skill throughout the observational period. These models, developed over the calibration period (1950–2020), were subsequently applied to ModE-RA paleo-reanalysis data (Valler et al., 2024) spanning 1421–2008, to infer the corresponding R10mm PCs. Finally, the spatial variability patterns of R10mm from the calibration period, in conjunction with the reconstructed PCs, were utilized to reconstruct the full R10mm anomaly field over the entire ModE-RA period (1421–2008). Further methodological details are provided in (Rimbu et al., 2025). To identify years characterized by reduced solar activity, we utilized the normalized time series of sunspot numbers spanning the period 1610–1950 (Hoyt and Schatten, 1998). The sun spot number timeseries has been compared to normalized flooding frequencies (i.e. number of floods per anno) represented by sediment core data from River Ammer (Czymzik et al., 2012; Czymzik et al., 2013). Years were classified as low solar activity years for the composite analysis if their normalized values fell below the threshold of –0.5 σ.

2.4 Rossby wave packets analysis

The frequency of Rossby wave packets (RWPs) is calculated using the functions implemented in the R package metR (Zimin et al., 2003). This method has already been succesfully used in numerous studys identifying the Northern Hemisphere storm track (Karami, 2019; Quinting and Vitart, 2019; Rimbu et al., 2024). We estimate the Amplitude of the Wave Packet envelope (WPA) by considering the 250 hPa meridional wind component (v) to describe deviations from the zonal flow. For each latitudinal circle of the N longitudinal points, the Fourier transform coefficients V_k of v have been calculated:

$$V_k = \frac{1}{N}\sum_{l=1}^{N} v(\frac{2\pi l}{N})\, e^{-\frac{2\pi i k l}{N}}, k = -\frac{N}{2}+1,\ldots,\frac{N}{2} \quad \text{(Eq. 1)}$$

Then the signal has been reconstructed through the inverse Fourier transform for the wave numbers typical of synoptic scale, that is, 4 to 1 as follows:

https://doi.org/10.5194/egusphere-2026-3630
Preprint. Discussion started: 9 July 2026

$$w(\tfrac{2\pi l}{N}) = 2\sum_{k=4}^{k=11} V_k e^{\frac{2\pi i k l}{N}} \quad \text{(Eq. 2)}$$

Finally, the WPA is estimated from the equation given below:

$$\mathrm{WPA}(\tfrac{2\pi l}{N}) = |\, w(\tfrac{2\pi l}{N}) \,|. \quad \text{(Eq. 3)}$$

The WPA is calculated at each grid point for summer days. A RWP is identified when the WPA at a given grid point exceeds 20 m/s. We then count the number of days on which this criterion is met and compare the resulting frequencies between the reference simulations and those assuming a GSM scenario.

2.5 Statistical Methods

To assess whether the solar signals in 2-meter temperature, 850 hPa air temperature, and geopotential height are statistically significant in the long-term mean (JJA and individual summer months), we apply a two-sided Student's t-test using the scipy.stats.ttest_ind() function in Python. To test whether the occurrence frequencies of RWPs and R10mm days differ significantly between scenarios, we use a χ^2 test as implemented in scipy.stats.chi2_contingency(). The North–South temperature and geopotential gradients are calculated by first computing area-weighted means over two regions of the North Atlantic sector: a northern box (90°N–70°N, 60°W–10°E) and a southern box (30°N–50°N, 60°W–10°E). The gradients are then obtained by subtracting the southern mean from the northern mean. Solar-induced signals in these quantities are determined by subtracting the values in the reference simulation from those in the GSM simulation for the respective periods.

3 Results

3.1 Climate fingerprints of Grand Solar Minima under contrasting background states

To analyze the long-term, state-dependent fingerprints of a GSM, we conducted paired simulations under preindustrial (PI) and late–21st-century (Future) high–greenhouse-gas-emission (SSP3-7.0 (Meinshausen et al., 2020)) conditions, including corresponding concentrations of ozone-depleting substances (ODS). Each set was performed with and without a strong MM–like reduction in total and spectral solar irradiance (TSI/SSI) (see Methods for details).

The June–July–August (JJA) mean 2-meter air temperature distributions under PI conditions (Fig. 1a) and the temperature anomalies under a future warming scenario (Fig. 1d), highlight well-established features of anthropogenic impacts such as stronger warming over land and amplified warming at high latitudes. In a GSM scenario (Figs. 1b and 1e), a global temperature reduction of −0.2 K under PI and −0.5 K under future atmospheric background conditions is simulated. The spatial expressions

https://doi.org/10.5194/egusphere-2026-3630
Preprint. Discussion started: 9 July 2026

also diverge. In the PI simulation, anomalies in the North Atlantic sector are heterogeneously distributed and modest at polar latitudes (Fig. 1c). Compared to that, polar cooling is five times larger (Fig. 1f) in the Future simulation, reflecting the direct coupling of irradiance changes with an ice-free ocean surface. In the following, we show that although the absolute thermal sensitivity to solar forcing increases in a warmer climatic background, its impact on weather dynamics becomes fundamentally weaker.

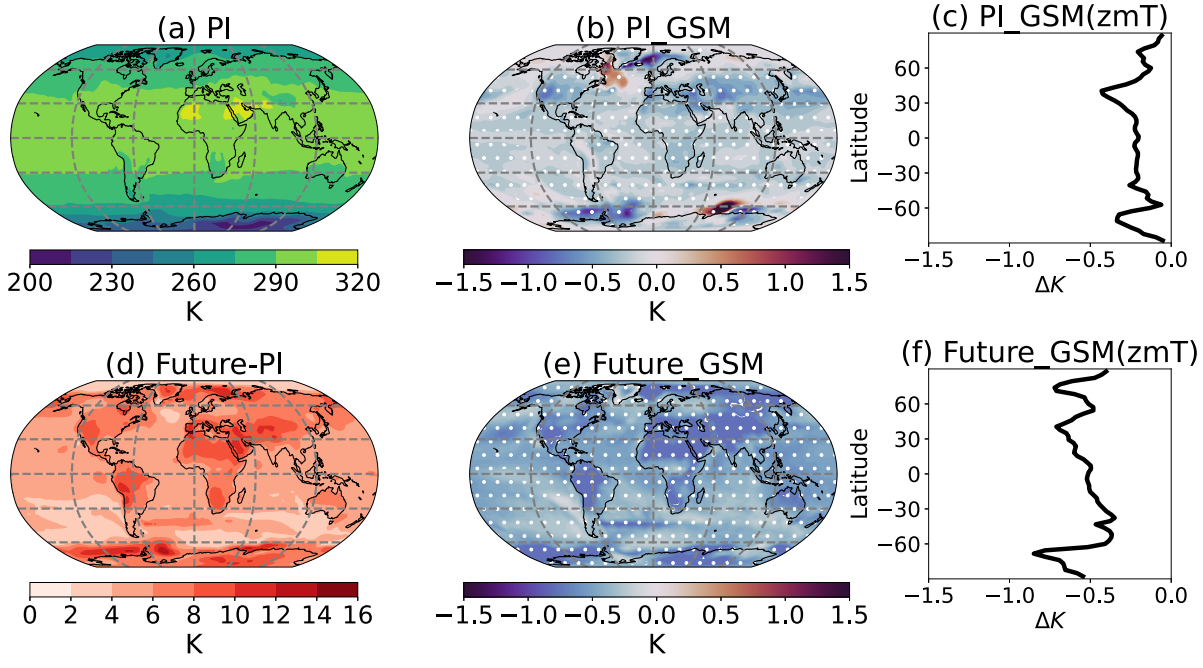

Figure 1. Global distribution of 2-meter air temperature under PI climate conditions (a), and projected anomalies under future global warming (d). Panels (b) and (e) show the 2-meter temperature offsets due to the influence of a GSM under PI and future climate conditions, respectively. (c) and (f) Zonal-mean 2-meter temperature offsets under PI and future climate conditions. All maps represent the June–July–August (JJA) seasonal mean. All Climate change anomalies are statistically significant at the 99% confidence level, while GSM-induced anomalies are significant at the 95% level.

3.2 Grand Solar Minima effectively modulate European summer extremes under PI climate conditions

Summer floods frequently affect the Alpine foreland, where heavy rainfall results from convective activity, abundant moisture, and orographic forcing along the northern Alps. Slow-moving low-pressure systems can amplify these conditions, as during the August 2005 flood. To investigate potential solar influences on such hydrological extremes and to disentangle the governing atmospheric dynamics (Beurton and Thieken, 2009; Fischer et al., 2022; Parajka et al., 2010) in past and future

https://doi.org/10.5194/egusphere-2026-3630
Preprint. Discussion started: 9 July 2026

climate states we analyze sediment records, meteorological reconstructions and tailor-made high complexity chemistry-climate model experiments.

Sediment records from the Ammer River, which is located in the Alpine foreland in southern Germany, reveal a clear anticorrelation between solar activity and flood frequency particularly during pronounced GSM phases (Fig. 2a), suggesting a solar influence on hydrological extremes.

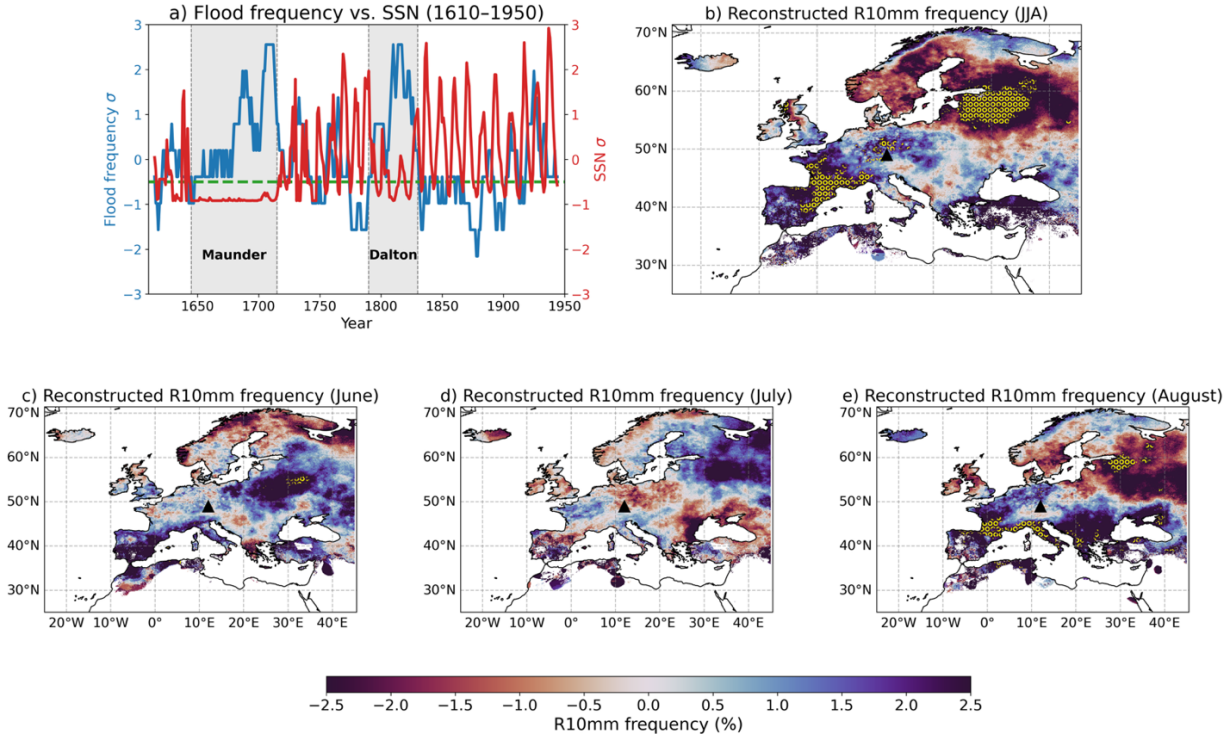

Figure 2. a) The normalized time series of sunspot numbers (SSN) and the flood frequency of the River Ammer The green horizontal line marks −0.5σ of the solar time series, defining the threshold for low solar activity composites. (b-e) Composite of the reconstructed R10mm index (frequency of days with ≥10 mm precipitation) during years of low solar activity**.** Dotted regions are significant at the 90% level. The triangle marker approximates the geographic location of the River Ammer (48.01°N, 11.12°E).

We first reconstruct the time series of the heavy-precipitation index (R10mm) based on the methodology described in Rimbu et al. (2025), before we compute composites for low–solar-intensity years between 1610 and 1949. The resulting spatial pattern reveals a dipole over Europe (Fig. 2b), with enhanced extremes from Western to Eastern Europe and parts of the Mediterranean, and suppressed activity at higher latitudes. The prevailing seasonal pattern is largely shaped in late summer (August; Fig. 2e).

https://doi.org/10.5194/egusphere-2026-3630
Preprint. Discussion started: 9 July 2026

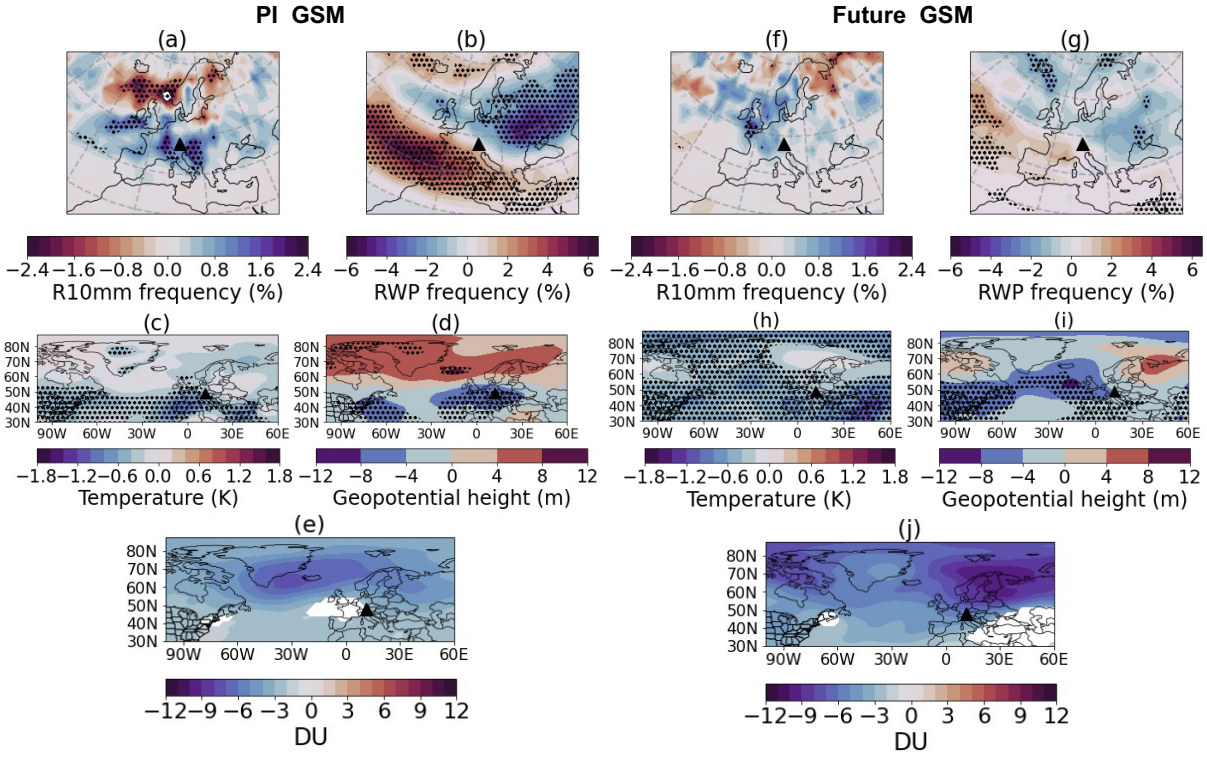

Figure 3. GSM-induced anomalies in a PI and Future climate state in the frequency of R10mm days, RWPs, temperature and geopotential height at 850 hPa and total ozone column (TOC) for late summer (August). Dotted regions are significant at the 95% level. Only those TOC anomalies significant at the 99% level are shown.

Our model integration that assumes a GSM under PI climate conditions (PI_GSM) reproduces the spatial fingerprints of extreme precipitation quite well (Fig. 3a). The experiment shows a robust increase in the frequency of R10mm days in a band from Western to Southeastern Europe, consistent with observed flood peaks in the Ammer River catchment during the Maunder and Dalton minima, and a decrease in the probability of R10mm days further north. The anomaly intensifies throughout the season (see Extended Data Fig. S1), with late summer (August) again showing the clearest pattern. Under future climate conditions, no clear or statistically significant pattern emerges (Fig. 3f and Extended Data Fig. S2).

https://doi.org/10.5194/egusphere-2026-3630
Preprint. Discussion started: 9 July 2026

To investigate the dynamical drivers of the observed extreme-precipitation pattern, we apply a RWP frequency tracking algorithm (Rimbu et al., 2024) to detect the position and intensity of storm tracks. The experiments without GSM forcing reproduce the North Atlantic maxima and realistic storm track positioning over Europe. Consistent with previous studies (Trevisiol et al., 2022), anthropogenic forcing weakens the storm track and shifts it northward over the European continent (Extended Data Fig. S3). GSM-induced anomalies in the PI setting (Fig. 3b) reveal a southward shift of the storm track mirrored in the pattern of extreme precipitation. This signal vanishes under future conditions (Fig. 3g), suggesting that anthropogenic warming masks the solar influence on extreme hydro-meteorological conditions. As already seen in the 2-meter temperature, the thermal response in the lower troposphere is much weaker (insignificant and even slightly positive locally) at high latitudes under PI conditions compared to the response under future conditions (compare Fig. 3c and 3h). Additionally, the GSM-induced anomalies in geopotential height in the PI climate state resemble characteristics of a negative phase of the Northern Annular Mode (NAM) at 850hPa and throughout the troposphere, whereas in a future warm climate no preferred phase dependence is evident (compare Fig. 3d and 3i, and Extended Data Fig. S4). It further shows that the configuration of temperature and geopotential height anomalies correlates with the strength of the anomalies in the TOC - that is, the strongest TOC anomalies occur in regions where temperatures are modestly negative or slightly positive and high-pressure conditions prevail. In the PI_GSM simulation, a pronounced negative ozone anomaly is established southward of Greenland stretching to subpolar latitudes (Fig 3e).

3.3 Linking solar forcing to summer extremes via sea-ice and ozone feedbacks

Our results trace the GSM-induced dynamical pattern under PI conditions to a chain of solar–cryospheric-radiative feedbacks that is projected to break down in a warmer climate, disrupting the pathways and fingerprints of solar activity over the North Atlantic. Our findings are summarized schematically in Figure 4.

https://doi.org/10.5194/egusphere-2026-3630
Preprint. Discussion started: 9 July 2026

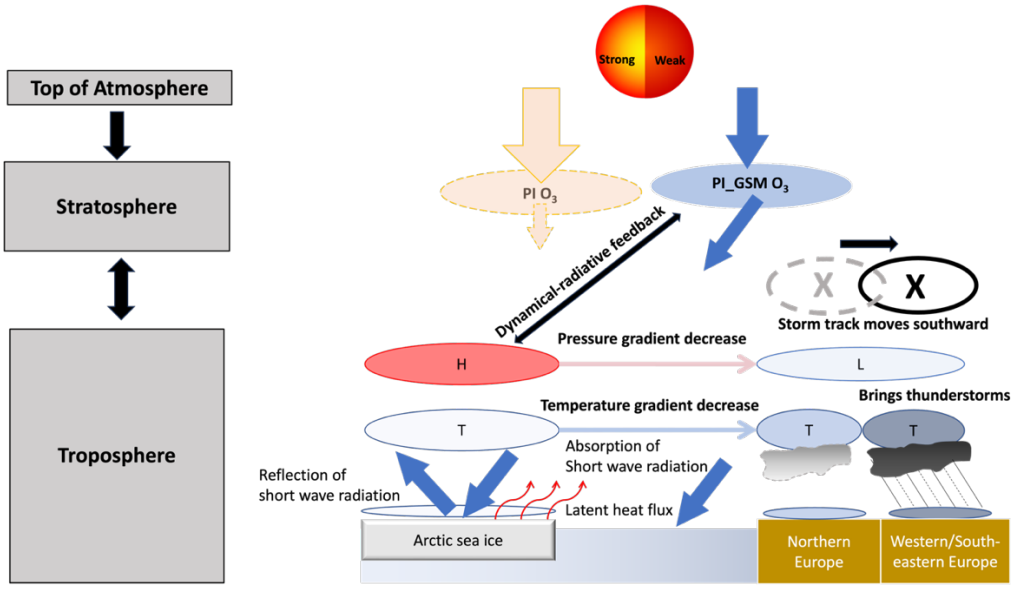

Figure 4. The Solar–Cryospheric Radiative Coupling (SCRC) mechanism under pre-industrial climate conditions and its impact on hydro-meteorological extremes in Europe. During a GSM, incoming shortwave solar radiation is substantially reduced (compare the width of blue and orange arrows at the top). This reduction decreases stratospheric ozone compared to regular PI conditions without a GSM (blue and orange ovals below the arrows), which in turn lowers the absorption of solar energy and partly compensates for the initial reduction in irradiance (compare arrow widths below the schematic ozone field). Over Arctic sea ice, reflected sunlight causes only a slight surface cooling, allowing for slightly thicker and more extensive sea ice and associated latent heat release (reddish curled arrows). Consequently, surface cooling over the Arctic remains modest (light blue oval). In contrast, over ice-free oceans, reduced solar absorption leads to stronger cooling. The resulting heterogeneous temperature response alters the meridional temperature gradients in the lower troposphere, leading to an adjustment in the geopotential height pattern. A relative high-pressure anomaly (H) develops over polar to subpolar latitudes, while a relative low (L) forms over mid- and subtropical regions. Under high-pressure influence, air masses become poorer in ozone, further reducing solar absorption and limiting polar to subpolar cooling even more. As a result, the temperature gradients in the transition zone between subpolar and mid-latitudes decrease, causing a destabilization and stronger meandering of storm tracks bringing enhanced precipitation in a band from Western to Southeastern Europe.

The GSM-induced spatial distribution of temperature anomalies under PI conditions—marked by a weak response at high latitudes and a stronger response at lower latitudes—stems from the high-albedo effect of persistent sea ice. The ice surface efficiently reflects much of the incoming shortwave radiation back to space, largely offsetting the reduction in solar input

https://doi.org/10.5194/egusphere-2026-3630
Preprint. Discussion started: 9 July 2026

during a GSM. Moreover, the intact sea-ice cover acts as a physical barrier that limits energy exchange between the atmosphere and the ocean, further suppressing GSM-induced surface cooling. As a result, the lower polar troposphere experiences only weak cooling, which nonetheless promotes slightly more extensive and thicker summer sea ice, enhancing freezing and latent heat release (Extended Data Figure S5) that again dampen GSM-induced cooling at high latitudes. As a consequence of the differential cooling, a relative high-pressure system develops at higher latitudes, while a relative low-pressure system is established in the mid- to subtropical latitudes. The altered pressure field initiates a coupled dynamical–chemical feedback with ozone, further modulating the spatial pattern of temperature anomalies over the North Atlantic.

During a GSM—the reduction in shortwave radiation—particularly at wavelengths below 240 nm—slows down chemical ozone production in the Chapman cycle, leading to a decrease in stratospheric ozone. While this determines the general sign of TOC anomalies, the prevailing atmospheric dynamics modulate the pattern. Tropospheric weather systems exert a well-documented influence on TOC variability. In high-pressure systems, subsiding air causes adiabatic warming in the lower troposphere, lifting the tropopause and lower stratosphere air masses. This upward displacement leads to adiabatic cooling aloft and brings ozone-poor air upward, reducing the TOC. Additionally, high-pressure systems suppress the horizontal transport of ozone-rich air from higher latitudes (Steinbrecht et al., 2003). During a GSM, these dynamically driven local ozone minima directly affect shortwave transmission through the atmosphere: reduced ozone concentrations lower absorption, allowing more shortwave radiation to reach the surface. As a result, surface cooling is most effectively suppressed where ozone depletion is strongest, across subpolar latitudes over the open North Atlantic. This suggests that radiative–chemical–dynamical feedbacks during a GSM can limit surface cooling in some regions, while acting as amplifiers in others. Notably, capturing such localized processes requires high-complexity chemistry–climate models with well-resolved radiation schemes and realistic representations of middle-atmosphere dynamics.

In summary, these feedback interactions weaken the meridional temperature and pressure gradients in the lower troposphere across the Atlantic, most strongly in the transition zone between the subpolar and mid-latitudes (~55° N). This leads to a wavier and less stable storm track, with enhanced meandering and more frequent southward excursions over Europe, bringing increased precipitation from Western to Southeastern Europe (Fig. 3c). It has been noted in earlier studies that the temperature gradient in the transition zone of the lower troposphere is of particular relevance for shaping the strength and location of the European summer storm track (Dong et al., 2013). Especially the significant increase in precipitation propagating from Northwestern to Eastern Europe is one of the features of a negative summer North Atlantic Oscillation (SNAO), which depends on the state of the NAM and correlates well with extreme weather conditions and floodings (Liu et al., 2025). Paleoclimate reconstructions of the summer SNAO further indicate that during colder periods, such as the Little Ice Age, a prevailing tendency toward a negative SNAO phase can be observed, thereby lending additional support to our findings (Linderholm & Folland 2017). However, since we are not computing composites for specific phases of the NAM or SNAO, and because additional dynamical processes are at play in our simulations, the solar-induced pattern in extreme precipitation is not completely identical with that of a negative SNAO.

https://doi.org/10.5194/egusphere-2026-3630
Preprint. Discussion started: 9 July 2026

The observed peak responses in August, in both reconstructions and model integrations, reflects several seasonal factors. First, the pattern needs time to fully develop (Extended Data Figure S4 column 1 and 2). Second, the climatological storm track maxima is closest to Europe in August (Extended Data Figure S1 column 1), making solar-induced shifts more regionally impactful. Third, generaly fewer heavy precipitation events enhance the visibility of GSM-induced anomalies (Extended Data Figure S1 column 3). Finally, by late summer, the insolation differences (GSM vs. REF) weaken as high latitude solar input declines after the solstice (Extended Data Figure S4 column 1).

In contrast, our GSM simulations under a high-emissions future show no such response. With the disappearance of summer sea ice, irradiance anomalies couple directly to the ocean mixed layer, leading to enhanced high-latitude cooling and more uniform conditions across the Atlantic. As a consequence, no distinct bipolar pressure anomalies develop—an essential prerequisite for a feedback between dynamics and ozone that, in the PI_GSM simulation, carries the signal from polar to subpolar latitudes and affects the meridional temperature gradients there. Furthermore, by 2100, the storm track transitions into a weaker mean state (Extended Data Fig. S3b), reducing the potential for solar-induced modulations in the opposite direction. Consequently, the distinct features in heavy precipitation vanish, and the GSM leaves no detectable fingerprint in summer extremes.

4 Conclusion

In this study we demonstrated that identical solar perturbations yield divergent hydroclimatic outcomes depending on period specific atmospheric background conditions. Our results show that reduced solar activity—as during the Maunder and Dalton Minima—amplified extreme summer precipitation from Western to Southeastern Europe through a coherent chain of processes involving sea ice, stratospheric ozone chemistry and storm track dynamics. This summer response to solar variability has been largely underappreciated, with most previous studies focusing on winter (Chiodo et al., 2019; Gray et al., 2010; Huo et al., 2025; Spiegl et al., 2023). Moreover, our findings demonstrate that solar imprints can manifest strikingly in daily weather extremes—not just in long-term climatological means.

It is important to emphasize that the Maunder and Dalton Minima were not affected by solar forcing anomalies alone. In particular, the Dalton Minimum overlapped with strong volcanic forcing, including the unidentified 1809 eruption, the 1815 Tambora eruption, and additional smaller to moderate eruptions in the early nineteenth century (Anet et al., 2014; Timmreck et al., 2021; Fang et al., 2023). Volcanic forcing also affected parts of the broader MM period and the Late MM, although its temporal structure differed from the clustered volcanic forcing around the Dalton Minimum (Luterbacher et al., 2001; Anet et al., 2014). Therefore, reconstructed hydroclimatic anomalies during the Maunder and Dalton Minima cannot be attributed uniquely to reduced solar activity. This limitation is particularly relevant when comparing idealized simulations with proxy records from historically forced periods.

https://doi.org/10.5194/egusphere-2026-3630
Preprint. Discussion started: 9 July 2026

Our experiments were not designed to reconstruct the full climate evolution of the Maunder or Dalton Minimum. Instead, they are idealized time-slice sensitivity experiments that isolate the hydroclimatic response to a strong reduction in solar irradiance under different background climate states. Volcanic forcing was therefore deliberately excluded to avoid mixing externally forced signals and to allow for a clean attribution of the simulated anomalies to the imposed solar perturbation. In this sense, comparisons with Maunder- and Dalton-era proxy records should be interpreted as consistency checks rather than as direct attribution of historical anomalies to solar forcing alone. More broadly, our results highlight that the climatic expression of an externally imposed radiative perturbation depends strongly on the background climate state. We therefore expect that volcanic forcing, or combined solar–volcanic forcing, may likewise produce different regional hydroclimatic fingerprints under different climatic backgrounds, although the specific mechanisms would not be identical because volcanic aerosols and solar irradiance changes affect radiation, chemistry, and dynamics in different ways.

The Ammer flood record was used here as an exemplary proxy archive from the northern Alpine foreland, where sedimentary flood layers provide a particularly sensitive record of past hydroclimatic extremes. We do not interpret this single archive as evidence for a spatially uniform European flood response to reduced solar activity. Rather, it serves as one regional consistency check for the modelled increase in heavy precipitation and flood-prone conditions over central Europe. Other flood reconstructions from the Alpine and central European domain likewise indicate pronounced hydroclimatic variability and, in some cases, enhanced flood activity during periods of reduced solar activity or Little Ice Age conditions, including records from the Bavarian Alpine Foreland and Alpine lake-sediment archives (Böhm et al., 2015; Czymzik et al., 2016; Peña et al., 2015; Schulte et al., 2015). Documentary flood reconstructions from the Upper Rhine and its tributaries show that flood occurrence in Central Europe is highly spatially structured and depends on catchment-specific meteorological triggers, supporting our interpretation that individual archives such as the Ammer record should be viewed as regional consistency checks rather than evidence for a uniform European response (Himmelsbach et al., 2015). Documentary and instrumental flood reconstructions from the High Rhine basin further show strong seasonal and multidecadal flood variability in the Alpine–Central European domain, with summer floods particularly frequent between 1651 and 1750, although this evidence is not an unambiguous attribution to solar forcing alone (Wetter et al., 2011). At the same time, not all European flood archives show the same sign of response. Swiss flood chronologies, for example, document phases of reduced flood frequency during parts of the Maunder and Dalton Minima, and historical flood series from other European regions emphasize strong spatial and seasonal heterogeneity (Schmocker-Fackel and Naef, 2010; Macdonald and Sangster, 2017). We therefore regard the proxy evidence as regionally differentiated rather than uniformly confirmatory. This is consistent with our model results, which show a spatially structured response with enhanced heavy precipitation from Western to Southeastern Europe and reduced activity further north. We expect that individual hydrological systems differ in their ability to record solar-related circulation changes, depending on catchment characteristics, seasonality, archive sensitivity, storm-track position, and the superposition of other forcings such as volcanic eruptions.

https://doi.org/10.5194/egusphere-2026-3630
Preprint. Discussion started: 9 July 2026

On the other hand our conclusions align with recent long-term reconstructions of human population dynamics that point to a connection between multicentennial solar variability and global demographic cycles throughout the Holocene (Wirtz et al., 2024). These reconstructions suggest that population growth oscillations across all inhabited continents followed multicentennial solar cycles and correlated not with mean climate conditions, but with their stability. In light of our results—demonstrating that GSMs amplified extreme summer precipitation in Europe through a coherent, state-dependent atmospheric mechanism—a consistent picture emerges: solar variability modulates short-term climate extremes in ways that can scale up to influence long-term societal dynamics, particularly when the background climate allows such variability to manifest in the circulation system.

Crucially, we demonstrate that the proposed mechanisms operate robustly under preindustrial climate conditions, but break down in a warmer future climate. As future climates increasingly diverge from past analogues, it becomes essential to consider not only the persistence of solar signals, but also how their fingerprints may change under different background conditions—both when interpreting paleoclimate records and when assessing future risks.

This interpretation is consistent with recent causal-inference analyses of Alpine flood variability, which suggest that solar irradiance can modulate preindustrial flood frequency through changes in summer atmospheric circulation, particularly the summer North Atlantic Oscillation, while these solar–flood relationships weaken under modern anthropogenic forcing (Peña-Rabadán et al., 2026). Although based on a different catchment and proxy framework, this study supports the broader view that solar-related hydroclimatic signals are not stationary in time, but depend on the prevailing climatic background state.

Additionally, our findings offer a new perspective on long-standing uncertainties regarding solar variability signals on decadal timescales, particularly the 11-year solar cycle. These signals have historically appeared weak and unstable across different segments of the instrumental record (1850–today). It has been suggested that stronger solar-cycle imprints in climatological means since the 1930s may reflect slightly higher solar-cycle amplitudes in the more recent period (Chiodo et al., 2019; Drews et al., 2022). Based on our results, we challenge this interpretation and argue instead that the improved detectability of solar-cycle signals since the 1930s also arises from anthropogenic climate change—which has altered the background state of the climate system in ways that amplify the thermal fingerprints of solar forcing in long-term climatological means, even as their dynamical imprints on weather extremes vanish in a greenhouse-gas-dominated world, as demonstrated in this study.

Here, we focused on the radiative–cryospheric pathway through which solar forcing can influence hydro-meteorological extremes. However, changes in other components of the climate system — such as volcanic aerosols, cloud feedbacks, ocean circulation, or polar vortex dynamics — may likewise modulate the manifestation of externally forced climate fingerprints under evolving background conditions. Identifying these additional pathways will be essential for achieving a more

https://doi.org/10.5194/egusphere-2026-3630
Preprint. Discussion started: 9 July 2026

comprehensive understanding of solar–climate interactions across different climatic epochs and, in particular, in a future warming world.

Appendix A

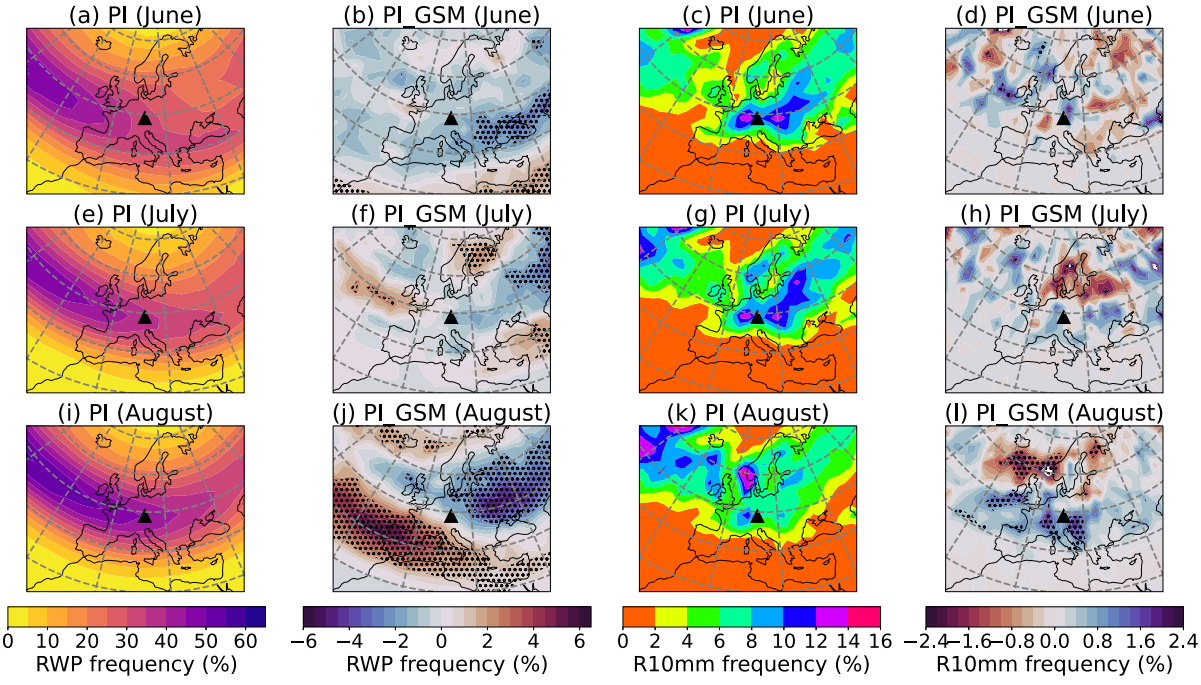

Figure A1. Intraseasonal distribution of RWP frequencies over the European sector under PI conditions (a, e, i) and anomalies induced by a GSM (b, f, j). Distribution of R10mm frequencies under PI conditions (c, g, k) and anomalies induced by a GSM (d, h, l). All significant anomalies (stippled areas) are shown at the 95% confidence.

https://doi.org/10.5194/egusphere-2026-3630
Preprint. Discussion started: 9 July 2026

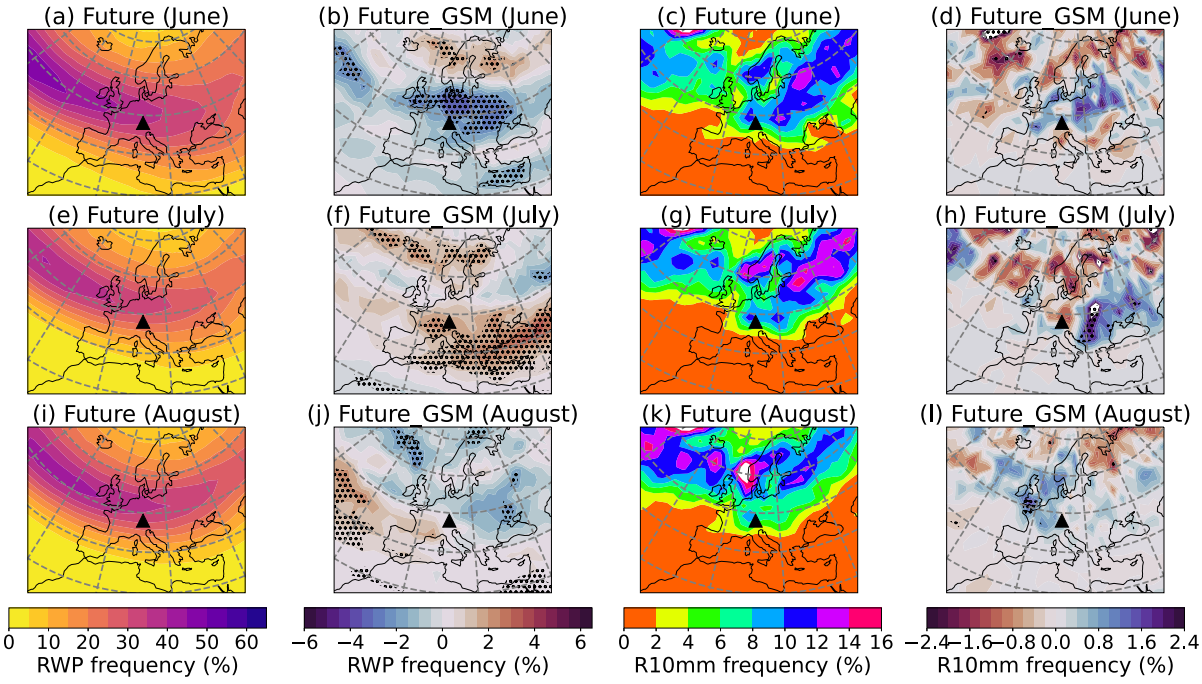

Figure A2. Like Figure S1 but under Futrue climate conditions.

400

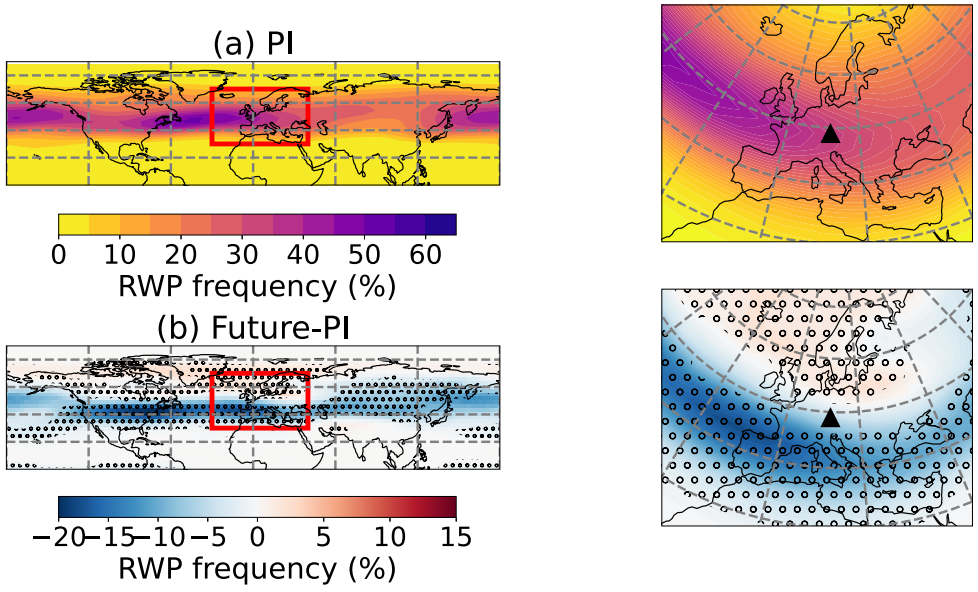

Figure A3. Northern Hemisphere distribution of RWP frequencies under PI climate conditions (a), and anomalies in RWP frequencies under future climate conditions (b). All maps represent the June–July–August (JJA) seasonal mean. All significant anomalies (stippled areas) represent the 95% confidence level.

https://doi.org/10.5194/egusphere-2026-3630
Preprint. Discussion started: 9 July 2026

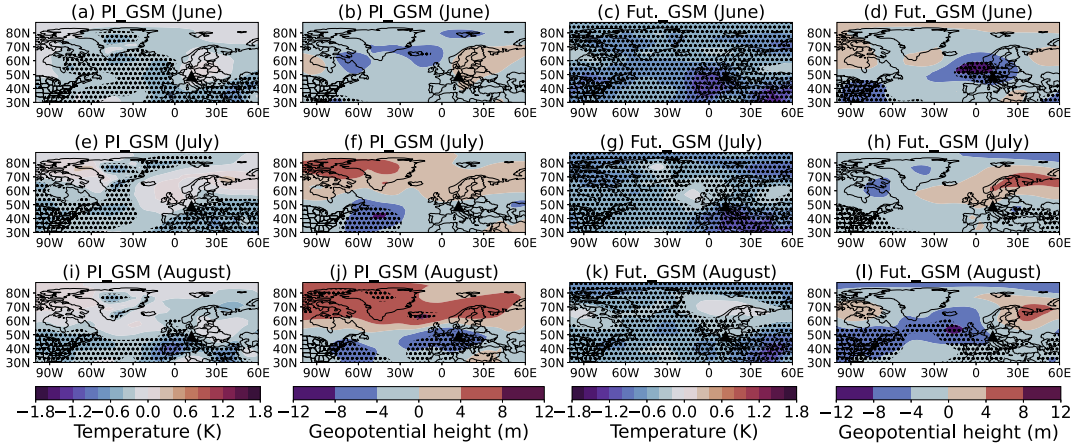

405

Figure A4. Intraseasonal anomalies induced by a GSM in 850 hPa air temperature and geopotential height under PI climate conditions (columns 1 and 2) and future climate conditions (columns 3 and 4). All significant anomalies (stippled areas) are shown at the 95% confidence level.

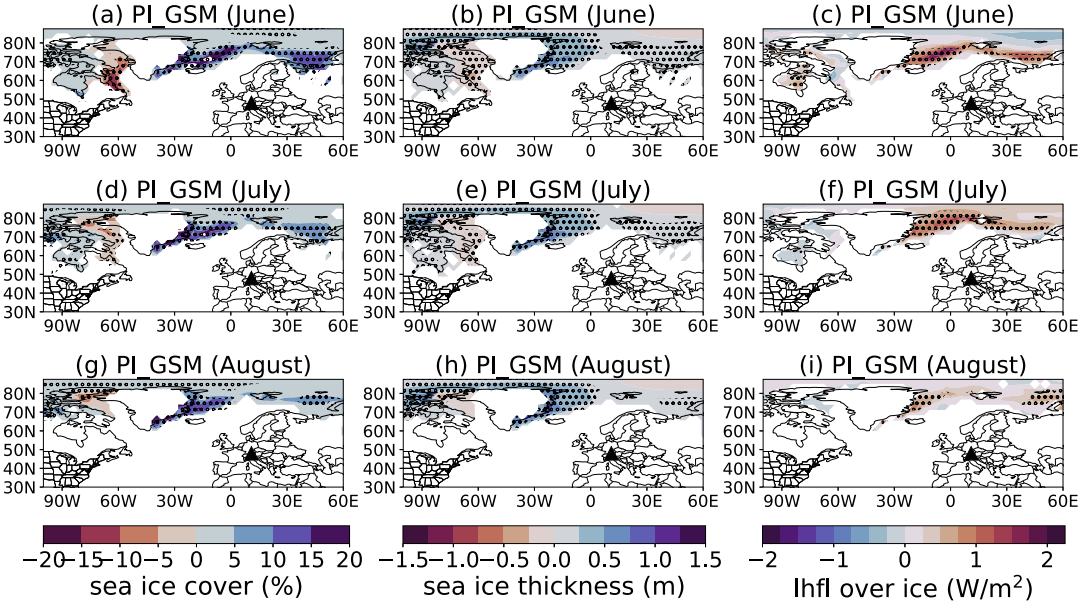

410

Figure A5. Intraseasonal anomalies induced by a GSM under PI conditions in sea ice cover (column 1), sea ice thickness (column 2) and latent heat flux (lhfl) (column 3). All significant anomalies (stippled areas) are shown at the 95% confidence level.

https://doi.org/10.5194/egusphere-2026-3630
Preprint. Discussion started: 9 July 2026

Code and data availability

Monthly data required to reproduce our analysis are publicly available from the German Climate Computing Center (DKRZ) (Spiegl et al., 2023). Due to storage limitations, additional data—including daily datasets—can be obtained upon reasonable request from the corresponding author. The EMAC model code is available upon request through the MESSy consortium (https://messy-interface.org/).

Author contributions

T.S. conceptualized the study, designed the experiments, conducted the simulations, performed the formal analysis, acquired funding, developed the methodology, prepared the visualizations, and wrote the original draft. N.R. contributed to the formal analysis, methodology, visualization, and writing – review and editing. F.K. conducted simulations and contributed to writing – review and editing. X.H., W.H., S.T., and U.L. contributed to writing – review and editing. G.L. contributed to the formal analysis, funding acquisition, methodology, writing – review and editing, and supervision.

Competing interests

G.L. is a member of the editorial board of Earth System Dynamics. All other authors do not have any potential conflicts of interest.

Disclaimer

Copernicus Publications remains neutral with regard to jurisdictional claims made in the text, published maps, institutional affiliations, or any other geographical representation in this paper. While Copernicus Publications makes every effort to include appropriate place names, the final responsibility lies with the authors. Views expressed in the text are those of the authors and do not necessarily reflect the views of the publisher.

Acknowledgements and financial support

This work was financially supported by the Helmholtz InnoPool project SOLVe (“SOLar and Volcanic Fingerprints in Past and Future Climates”) (https://earthenvironment.helmholtz.de/changing-earth/de/innopool-projects) and the BMBF project ReKlim (EP36660030). We would also like to thank the BMBF SOLCHECK project (“Solar Contributions to Climate Change on Decadal to Centennial Timescales”) (01LG1906B) for providing the data that form the basis of our analysis. We further

https://doi.org/10.5194/egusphere-2026-3630
Preprint. Discussion started: 9 July 2026

thank the NHR-ZIB (Berlin) for granting computational resources for the SOLCHECK simulations. Finally, we would like to thank Dr. Tatiana Egorova (PMOD/WRC) for kindly providing the GSM solar forcing data used in our model integrations.

References

Ahmed, M., Anchukaitis, K. J., Asrat, A., Borgaonkar, H. P., Braida, M., Buckley, B. M., Büntgen, U., Chase, B. M., Christie, D. A., Cook, E. R., and Curran, M. A.: Continental-scale temperature variability during the past two millennia, Nat. Geosci., 6, 339–346, https://doi.org/10.1038/ngeo1797, 2013.

Anet, J. G., Rozanov, E., Muthers, S., Peter, T., Brönnimann, S., Arfeuille, F., Beer, J., Shapiro, A. I., Raible, C. C., Steinhilber, F., and Schmutz, W.: Impact of a potential 21st century "grand solar minimum" on surface temperatures and stratospheric ozone, Geophys. Res. Lett., 40, 4420–4425, https://doi.org/10.1002/grl.50806, 2013.

Anet, J. G., Muthers, S., Rozanov, E., Raible, C. C., Stenke, A., Shapiro, A. I., Brönnimann, S., Arfeuille, F. X., Brugnara, Y., Beer, J., Steinhilber, F., Schmutz, W., and Peter, T.: Impact of solar versus volcanic activity variations on tropospheric temperatures and precipitation during the Dalton Minimum, Clim. Past, 10, 921–938, https://doi.org/10.5194/cp-10-921-2014, 2014.

Arsenovic, P., Rozanov, E., Anet, J. G., Stenke, A., Schmutz, W., and Peter, T.: Implications of potential future grand solar minimum for ozone layer and climate, Atmos. Chem. Phys., 18, 3469–3483, https://doi.org/10.5194/acp-18-3469-2018, 2018.

Beurton, S. and Thieken, A. H.: Seasonality of floods in Germany, Hydrol. Sci. J., 54, 62–76, https://doi.org/10.1623/hysj.54.1.62, 2009.

Böhm, O., Jacobeit, J., Glaser, R., and Wetzel, K.-F.: Flood sensitivity of the Bavarian Alpine Foreland since the late Middle Ages in the context of internal and external climate forcing factors, Hydrol. Earth Syst. Sci., 19, 4721–4734, https://doi.org/10.5194/hess-19-4721-2015, 2015.

Campitelli, E.: metR: Tools for easier analysis of meteorological fields, R package version v0.14.0 [software], https://doi.org/10.5281/zenodo.2593516, 2021.

https://doi.org/10.5194/egusphere-2026-3630
Preprint. Discussion started: 9 July 2026

Chiodo, G., Oehrlein, J., Polvani, L. M., Fyfe, J. C., and Smith, A. K.: Insignificant influence of the 11-year solar cycle on the North Atlantic Oscillation, Nat. Geosci., 12, 94–99, https://doi.org/10.1038/s41561-018-0293-3, 2019.

Coddington, O., Lean, J., Pilewskie, P., Snow, M., Richard, E., Kopp, G., and Baranyi, T.: Solar irradiance variability: comparisons of models and measurements, Earth Space Sci., 6, 2525–2555, https://doi.org/10.1029/2019EA000693, 2019.

Cornes, R. C., van der Schrier, G., van den Besselaar, E. J., and Jones, P. D.: An ensemble version of the E-OBS temperature and precipitation data sets, J. Geophys. Res.-Atmos., 123, 9391–9409, https://doi.org/10.1029/2017JD028200, 2018.

Czymzik, M., Brauer, A., Dulski, P., Plessen, B., Naumann, R., von Grafenstein, U., and Scheffler, R.: Flood layer data from Ammersee sediment profile AS10prox, PANGAEA [data set], https://doi.org/10.1594/PANGAEA.803368, 2012.

Czymzik, M., Brauer, A., Dulski, P., Plessen, B., Naumann, R., von Grafenstein, U., and Scheffler, R.: Orbital and solar forcing of shifts in Mid-to Late Holocene flood intensity from varved sediments of pre-alpine Lake Ammersee (southern Germany), Quaternary Sci. Rev., 61, 96–110, https://doi.org/10.1016/j.quascirev.2012.11.010, 2013.

Czymzik, M., Muscheler, R., and Brauer, A.: Solar modulation of flood frequency in central Europe during spring and summer on interannual to multi-centennial timescales, Clim. Past, 12, 799–805, https://doi.org/10.5194/cp-12-799-2016, 2016.

De Jager, C., Akasofu, S. I., Duhau, S., Livingston, W. C., Nieuwenhuijzen, H., and Potgieter, M. S.: A remarkable recent transition in the solar dynamo, Space Sci. Rev., 201, 109–145, https://doi.org/10.1007/s11214-016-0293-9, 2016.

Dong, B., Sutton, R. T., Woollings, T., and Hodges, K.: Variability of the North Atlantic summer storm track: mechanisms and impacts on European climate, Environ. Res. Lett., 8, 034037, https://doi.org/10.1088/1748-9326/8/3/034037, 2013.

Drews, A., Huo, W., Matthes, K., Kodera, K., and Kruschke, T.: The Sun's role in decadal climate predictability in the North Atlantic, Atmos. Chem. Phys., 22, 7893–7904, https://doi.org/10.5194/acp-22-7893-2022, 2022.

Dunn, R. J. H., Alexander, L. V., Donat, M. G., Zhang, X., Bador, M., Herold, N., Lippmann, T., Allan, R., Aguilar, E., Barry, A. A., Brunet, M., Caesar, J., Chagnaud, G., Cheng, V., Cinco, T., Durre, I., de Guzman, R., Htay, T. M., Wan Ibadullah, W. M., Bin Ibrahim, M. K. I., Khoshkam, M., Kruger, A., Kubota, H., Leng, T. W., Lim, G., Li-Sha, L., Marengo, J., Mbatha, S., McGree, S., Menne, M., de los Milagros Skansi, M., Ngwenya, S., Nkrumah, F., Oonariya, C., Pabon-Caicedo, J. D., Panthou, G., Pham, C., Rahimzadeh, F., Rodriguez, L., Salinger, J., Sané, Y., Sopaheluwakan, A., Srivastava, A., Sun, Y., Timbal, B., Trachow, N., Trewin, B., van der Schrier, G., Vazquez-Aguirre, J., Vasquez, R., Villarroel, C.,

https://doi.org/10.5194/egusphere-2026-3630
Preprint. Discussion started: 9 July 2026

Vincent, L., Vischel, T., Vose, R., Bin Hj Yussof, M. N. A., and Zhai, P.: Development of an updated global land in situ-based data set of temperature and precipitation extremes: HadEX3, J. Geophys. Res.-Atmos., 125, e2019JD032263, https://doi.org/10.1029/2019JD032263, 2020.

Eddy, J. A.: The Maunder Minimum, Science, 192, 1189–1202, https://doi.org/10.1126/science.192.4245.1189, 1976.

Egorova, T., Schmutz, W., Rozanov, E., Shapiro, A. I., Usoskin, I., Beer, J., and Peter, T.: Revised historical solar irradiance forcing, Astron. Astrophys., 615, A85, https://doi.org/10.1051/0004-6361/201731199, 2018.

Fang, S.-W., Timmreck, C., Zanchettin, D., and Jungclaus, J. H.: On the additivity of climate responses to the volcanic and solar forcing in the early 19th century, Earth Syst. Dynam., 13, 1535–1559, https://doi.org/10.5194/esd-13-1535-2022, 2022.

Fang, S.-W., Timmreck, C., Muthers, S., Toohey, M., and Krüger, K.: The role of small to moderate volcanic eruptions in the early 19th century climate, Geophys. Res. Lett., 50, e2023GL105307, https://doi.org/10.1029/2023GL105307, 2023.

Feulner, G. and Rahmstorf, S.: On the effect of a new grand minimum of solar activity on the future climate on Earth, Geophys. Res. Lett., 37, L05707, https://doi.org/10.1029/2010GL042710, 2010.

Fischer, S., Lun, D., Schumann, A. H., and Blöschl, G.: Detecting flood-type-specific flood-rich and flood-poor periods in peaks-over-threshold series with application to Bavaria (Germany), Stoch. Environ. Res. Risk Assess., 37, 2127–2145, https://doi.org/10.1007/s00477-022-02350-8, 2022.

Funke, B., López-Puertas, M., Stiller, G. P., Versick, S., and von Clarmann, T.: A semi-empirical model for mesospheric and stratospheric NOy produced by energetic particle precipitation, Atmos. Chem. Phys., 16, 8667–8693, https://doi.org/10.5194/acp-16-8667-2016, 2016.

Ghazi, B., Przybylak, R., Oliński, P., and Pospieszyńska, A.: Flood occurrences and characteristics in Poland (Central Europe) in the last millennium, Global Planet. Change, 246, 104706, https://doi.org/10.1016/j.gloplacha.2025.104706, 2025.

Giorgetta, M. A. and Bengtsson, L.: Potential role of the quasi-biennial oscillation in the stratosphere-troposphere exchange as found in water vapor in general circulation model experiments, J. Geophys. Res.-Atmos., 104, 6003–6019, https://doi.org/10.1029/1998JD200120, 1999.

https://doi.org/10.5194/egusphere-2026-3630
Preprint. Discussion started: 9 July 2026

Gray, L. J., Beer, J., Geller, M., Haigh, J. D., Lockwood, M., Matthes, K., and White, W.: Solar influences on climate, Rev. Geophys., 48, RG4001, https://doi.org/10.1029/2009RG000282, 2010.

Himmelsbach, I., Glaser, R., Schoenbein, J., Riemann, D., and Martin, B.: Reconstruction of flood events based on documentary data and transnational flood risk analysis of the Upper Rhine and its French and German tributaries since AD 1480, Hydrol. Earth Syst. Sci., 19, 4149–4164, https://doi.org/10.5194/hess-19-4149-2015, 2015.

Hoyt, D. V. and Schatten, K. H.: Group sunspot numbers: A new solar activity reconstruction, Sol. Phys., 179, 189–219, https://doi.org/10.1023/A:1005007527816, 1998.

Huo, W., Spiegl, T., Wahl, S., Matthes, K., Langematz, U., Pohlmann, H., and Kröger, J.: Assessment of the 11-year solar cycle signals in the middle atmosphere during boreal winter with multiple-model ensemble simulations, Atmos. Chem. Phys., 25, 2589–2612, https://doi.org/10.5194/acp-25-2589-2025, 2025.

Ineson, S., Maycock, A. C., Gray, L. J., Scaife, A. A., Dunstone, N. J., Harder, J. W., Knight, J. R., Lockwood, M., Manners, J. C., and Wood, R. A.: Regional climate impacts of a possible future grand solar minimum, Nat. Commun., 6, 7535, https://doi.org/10.1038/ncomms8535, 2015.

Jungclaus, J. H., Keenlyside, N., Botzet, M., Haak, H., Luo, J. J., Latif, M., and Roeckner, E.: Ocean circulation and tropical variability in the coupled model ECHAM5/MPI-OM, J. Climate, 19, 3952–3972, https://doi.org/10.1175/JCLI3815.1, 2006.

Jöckel, P., Kerkweg, A., Pozzer, A., Sander, R., Tost, H., Riede, H., and Kern, B.: Development cycle 2 of the modular earth submodel system (MESSy2), Geosci. Model Dev., 3, 717–752, https://doi.org/10.5194/gmd-3-717-2010, 2010.

Jöckel, P., Tost, H., Pozzer, A., Kunze, M., Kirner, O., Brenninkmeijer, C. A. M., and Zahn, A.: Earth system chemistry integrated modelling (ESCiMo) with the modular earth submodel system (MESSy) version 2.51, Geosci. Model Dev., 9, 1153–1200, https://doi.org/10.5194/gmd-9-1153-2016, 2016.

Karami, K.: Upper tropospheric Rossby wave packets: Long-term trends and variability, Theor. Appl. Climatol., 138, 527–540, https://doi.org/10.1007/s00704-019-02845-5, 2019.

https://doi.org/10.5194/egusphere-2026-3630
Preprint. Discussion started: 9 July 2026

Kunze, M., Godolt, M., Langematz, U., Grenfell, J. L., Hamann-Reinus, A., and Rauer, H.: Investigating the early Earth faint young Sun problem with a general circulation model, Planet. Space Sci., 98, 77–92, https://doi.org/10.1016/j.pss.2013.09.011, 2014.

Linderholm, H. W. and Folland, C. K.: Summer North Atlantic Oscillation (SNAO) variability on decadal to palaeoclimate time scales, Past Global Changes Magazine, 25, 57–60, https://doi.org/10.22498/pages.25.1.57, 2017.

Liu, Q., Bader, J., Jungclaus, J. H., and Matei, D.: More extreme summertime North Atlantic Oscillation under climate change, Commun. Earth Environ., 6, 474, https://doi.org/10.1038/s43247-025-02422-x, 2025.

Luterbacher, J., Rickli, R., Xoplaki, E., Tinguely, C., Beck, C., Pfister, C., and Wanner, H.: The late Maunder minimum (1675–1715) – a key period for studying decadal scale climatic change in Europe, Climatic Change, 49, 441–462, https://doi.org/10.1023/A:1010667524422, 2001.

Macdonald, N. and Sangster, H.: High-magnitude flooding across Britain since AD 1750, Hydrol. Earth Syst. Sci., 21, 1631–1650, https://doi.org/10.5194/hess-21-1631-2017, 2017.

Matthes, K., Funke, B., Andersson, M. E., Barnard, L., Beer, J., Charbonneau, P., and Versick, S.: Solar forcing for CMIP6 (v3.2), Geosci. Model Dev., 10, 2247–2302, https://doi.org/10.5194/gmd-10-2247-2017, 2017.

Maycock, A. C., Ineson, S., Gray, L. J., Scaife, A. A., Anstey, J. A., Yiu, Y. Y., and Harder, J. W.: Possible impacts of a future grand solar minimum on climate: stratospheric and global circulation changes, J. Geophys. Res.-Atmos., 120, 9043–9058, https://doi.org/10.1002/2014JD022022, 2015.

Meehl, G. A., Arblaster, J. M., and Marsh, D. R.: Could a future "Grand Solar Minimum" like the Maunder Minimum stop global warming?, Geophys. Res. Lett., 40, 1789–1793, https://doi.org/10.1002/grl.50361, 2013.

Meinshausen, M., Nicholls, Z. R., Lewis, J., Gidden, M. J., Vogel, E., Freund, M., and Wang, R. H.: The shared socio-economic pathway (SSP) greenhouse gas concentrations and their extensions to 2500, Geosci. Model Dev., 13, 3571–3605, https://doi.org/10.5194/gmd-13-3571-2020, 2020.

Miyahara, H., Tokanai, F., Moriya, T., Takeyama, M., Sakurai, H., Horiuchi, K., and Hotta, H.: Gradual onset of the Maunder Minimum revealed by high-precision carbon-14 analyses, Sci. Rep., 11, 5482, https://doi.org/10.1038/s41598-021-84830-5, 2021.

https://doi.org/10.5194/egusphere-2026-3630
Preprint. Discussion started: 9 July 2026

Parajka, J., Kohnová, S., Bálint, G., Barbuc, M., Borga, M., Claps, P., Gaume, E., Hlavčová, K., Merz, R., Pfaundler, M., Stancalie, G., Szolgay, J., and Blöschl, G.: Seasonal characteristics of flood regimes across the Alpine–Carpathian range, J. Hydrol., 394, 78–89, https://doi.org/10.1016/j.jhydrol.2010.05.015, 2010.

Peña, J. C., Schulte, L., Badoux, A., Barriendos, M., and Barrera-Escoda, A.: Influence of solar forcing, climate variability and modes of low-frequency atmospheric variability on summer floods in Switzerland, Hydrol. Earth Syst. Sci., 19, 3807–3827, https://doi.org/10.5194/hess-19-3807-2015, 2015.

Peña-Rabadán, J. C., Schulte, L., Miró-Cubells, J. R., Casellas-Masana, E., and Carvalho, F.: Causal drivers of alpine flood variability from 1300 to 2020 revealed by climate time series analysis, EGUsphere [preprint], 2026, 1–23, https://doi.org/10.5194/egusphere-2026-303, 2026.

Quinting, J. F. and Vitart, F.: Representation of synoptic-scale Rossby wave packets and blocking in the S2S prediction project database, Geophys. Res. Lett., 46, 1070–1078, https://doi.org/10.1029/2018GL081381, 2019.

Rimbu, N., Ionita, M., Spiegl, T., and Lohmann, G.: Reconstruction of a Two-Dimensional Blocking Index During the Last Four Hundred Years Using Gridded Temperature and Precipitation Data, Atmosphere, 16, 477, https://doi.org/10.3390/atmos16040477, 2025.

Rimbu, N., Spiegl, T., Ionita, M., Doshi, S., and Lohmann, G.: A synoptic scale perspective of solar forcing on extreme precipitation and floods over Europe during summer, J. Geophys. Res.-Atmos., 129, e2024JD041952, https://doi.org/10.1029/2024JD041952, 2024.

Roeckner, E., Brokopf, R., Esch, M., Giorgetta, M. A., Hagemann, S., Kornblueh, L., and Schulzweida, U.: Sensitivity of simulated climate to horizontal and vertical resolution in the ECHAM5 atmosphere model, J. Climate, 19, 3771–3791, https://doi.org/10.1175/JCLI3824.1, 2006.

Rustemeier, E., Hänsel, S., Finger, P., Schneider, U., and Ziese, M.: GPCC Climatology Version 2022 at 2.5°: Monthly Land-Surface Precipitation Climatology for Every Month and the Total Year from Rain-Gauges Built on GTS-Based and Historical Data, available at: https://opendata.dwd.de/climate_environment/GPCC/html/gpcc_normals_v2022_doi_download.html (last access: 15 October 2024), 2022.

https://doi.org/10.5194/egusphere-2026-3630
Preprint. Discussion started: 9 July 2026

Sander, R., Baumgaertner, A., Gromov, S., Harder, H., Jöckel, P., Kerkweg, A., and Xie, Z. Q.: The atmospheric chemistry box model CAABA/MECCA-3.0, Geosci. Model Dev., 4, 373–380, https://doi.org/10.5194/gmd-4-373-2011, 2011.

Sander, R., Jöckel, P., Kirner, O., Kunert, A. T., Landgraf, J., and Pozzer, A.: The photolysis module JVAL-14, compatible with the MESSy standard, and the JVal PreProcessor (JVPP), Geosci. Model Dev., 7, 2653–2662, https://doi.org/10.5194/gmd-7-2653-2014, 2014.

Schmocker-Fackel, P. and Naef, F.: Changes in flood frequencies in Switzerland since 1500, Hydrol. Earth Syst. Sci., 14, 1581–1594, https://doi.org/10.5194/hess-14-1581-2010, 2010.

Schulte, L., Peña, J. C., Carvalho, F., Schmidt, T., Julià, R., Llorca, J., and Veit, H.: A 2600-year history of floods in the Bernese Alps, Switzerland: frequencies, mechanisms and climate forcing, Hydrol. Earth Syst. Sci., 19, 3047–3072, https://doi.org/10.5194/hess-19-3047-2015, 2015.

Sedlacek, J., Sukhodolov, T., Egorova, T., Karagodin-Doyennel, A., and Rozanov, E.: Future Climate Under CMIP6 Solar Activity Scenarios, Earth Space Sci., 10, e2022EA002783, https://doi.org/10.1029/2022EA002783, 2023.

Slivinski, L. C., Compo, G. P., Whitaker, J. S., Sardeshmukh, P. D., Giese, B. S., McColl, C., Allan, R., Yin, X., Vose, R., Titchner, H., Kennedy, J., Spencer, L. J., Ashcroft, L., Bronnimann, S., Brunet, M., Camuffo, D., Cornes, R., Cram, T. A., Crouthamel, R., Domínguez-Castro, F., Freeman, J. E., Gergis, J., Hawkins, E., Jones, P. D., Jourdain, S., Kaplan, A., Kubota, H., Le Blancq, F., Lee, T.-C., Lorrey, A., Luterbacher, J., Maugeri, M., Mock, C. J., Moore, G. W. K., Przybylak, R., Pudmenzky, C., Reason, C., Slonosky, V. C., Smith, C. A., Tinz, B., Trewin, B., Valente, M. A., Wang, X. L., Wilkinson, C., Wood, K., and Wyszynski, P.: Towards a more reliable historical reanalysis: improvements for version 3 of the Twentieth Century Reanalysis system, Q. J. Roy. Meteor. Soc., 145, 2876–2908, https://doi.org/10.1002/qj.3598, 2019.

Spiegl, T. C., Langematz, U., Pohlmann, H., and Kröger, J.: A critical evaluation of decadal solar cycle imprints in the MiKlip historical ensemble simulations, Weather Clim. Dynam., 4, 789–807, https://doi.org/10.5194/wcd-4-789-2023, 2023.

Spiegl, T. and Langematz, U.: Twenty-first-century climate change hot spots in the light of a weakening Sun, J. Climate, 33, 3431–3447, https://doi.org/10.1175/JCLI-D-19-0059.1, 2020.

https://doi.org/10.5194/egusphere-2026-3630
Preprint. Discussion started: 9 July 2026

Spiegl, T., Wahl, S., Huo, W., Schmidt, F., and Langematz, U.: ROMIC-II-SOLCHECK joint database part II – Grand Solar Minimum sensitivity experiments under different climatic background, [CHECK DATASET DETAILS], 2023.

Steinbrecht, W., Hassler, B., Claude, H., Winkler, P., and Stolarski, R. S.: Global distribution of total ozone and lower stratospheric temperature variations, Atmos. Chem. Phys., 3, 1421–1438, https://doi.org/10.5194/acp-3-1421-2003, 2003.

Timmreck, C., Toohey, M., Zanchettin, D., Sigl, M., Ludlow, F., Wilson, R., Stoffel, M., Oppenheimer, C., Büntgen, U., and Hegerl, G.: The unidentified eruption of 1809: a climatic cold case, Clim. Past, 17, 1455–1482, https://doi.org/10.5194/cp-17-1455-2021, 2021.

Trevisiol, A., Gilli, L., and Faggian, P.: Short and long-term projections of Rossby wave packets and blocking events with particular attention to the northern hemisphere, Global Planet. Change, 209, 103750, https://doi.org/10.1016/j.gloplacha.2022.103750, 2022.

Usoskin, I. G., Solanki, S. K., and Kovaltsov, G. A.: Grand minima and maxima of solar activity: New observational constraints, Astron. Astrophys., 471, 301–309, https://doi.org/10.1051/0004-6361:20077704, 2007.

Valler, V., Franke, J., Brugnara, Y., Samakinwa, E., Hand, R., Lundstad, E., and Brönnimann, S.: ModE-RA: a global monthly paleo-reanalysis of the modern era 1421 to 2008, Sci. Data, 11, 36, https://doi.org/10.1038/s41597-023-02733-8, 2024.

von Storch, H. and Zwiers, F. W.: Statistical analysis in climate research, Cambridge University Press, 2002.

Vose, R. S., Huang, B., Yin, X., Arndt, D., Easterling, D. R., Lawrimore, J. H., and Zhang, H. M.: Implementing full spatial coverage in NOAA's global temperature analysis, Geophys. Res. Lett., 48, e2020GL090873, https://doi.org/10.1029/2020GL090873, 2021.

Wetter, O., Pfister, C., Weingartner, R., Luterbacher, J., Reist, T., and Trösch, J.: The largest floods in the High Rhine basin since 1268 assessed from documentary and instrumental evidence, Hydrol. Sci. J., 56, 733–758, https://doi.org/10.1080/02626667.2011.583613, 2011.

Wirtz, K. W., Antunes, N., Diachenko, A., Laabs, J., Lemmen, C., Lohmann, G., and Gronenborn, D.: Multicentennial cycles in continental demography synchronous with solar activity and climate stability, Nat. Commun., 15, 10248, https://doi.org/10.1038/s41467-024-54474-w, 2024.

https://doi.org/10.5194/egusphere-2026-3630
Preprint. Discussion started: 9 July 2026

Zimin, A. V., Sznuyogh, I., Patil, D. J., Hunt, B. R., and Ott, E.: Extracting envelopes of Rossby wave packets, Mon. Weather Rev., 131, 1011–1017, https://doi.org/10.1175/1520-0493(2003)131<1011:EEORWP>2.0.CO;2, 2003.

Zolotova, N. V. and Ponyavin, D. I.: Is the new Grand minimum in progress?, J. Geophys. Res.-Space, 119, 3281–3285, https://doi.org/10.1002/2013JA019751, 2014.